American Mineralogist, Volume 107, pages 1643–1651, 2022

A revised analysis of ferrihydrite at liquid helium temperature using Mössbauer spectroscopy

James M. Byrne[1,*] and Andreas Kappler[2,3]

[1]School of Earth Sciences, University of Bristol, Wills Memorial Building, Queens Road, Bristol, BS8 1RJ, U.K.
[2]Geomicrobiology, Center for Applied Geosciences, University of Tuebingen, Schnarrenbergstrasse 94-96, 72076 Tübingen, Germany
[3]Cluster of Excellence: EXC 2124: Controlling Microbes to Fight Infections, 72074 Tübingen, Germany

Abstract

Short-range-ordered Fe(III) minerals such as ferrihydrite (Fh) are ubiquitous in the environment, are key players in biogeochemical cycling, and sorb trace elements and nutrients. As such, it is important to be able to identify the presence of such minerals in natural samples. Fh is commonly observed to be X-ray amorphous and cannot be easily analyzed using X-ray diffraction, meaning that spectroscopic methods such as X-ray absorption or ^{57}Fe Mössbauer spectroscopy (MBS) are necessary for accurate identification and quantification. Despite decades of research into Fh using MBS, there is a discrepancy in the literature about the exact parameters applicable to the mineral when measured at liquid helium temperature. Fh is frequently fitted with either one, two, or three hyperfine sextets with little interpretation applied to the meaning of each, which is problematic as a one sextet model does not account for the asymmetric lineshape frequently observed for Fh. Here, we address inconsistencies in the fitting of Fh and provide a more standardized approach to its identification by MBS. We present a systematic comparison of different fitting methods, notably based on Lorentzian and Voigt functions. We suggest that the most suitable approach to fitting pure Fh at liquid helium temperature is with two sextets (A and B) fitted using an extended Voigt-based function with the ability to apply probability distributions to each hyperfine parameter. 2-line Fh: A (δ = 0.49 mm/s; ε = 0.00 mm/s; B_{hf} = 50.1 T) and B (δ = 0.42 mm/s; ε = –0.01 mm/s; B_{hf} = 46.8 T) 6-line Fh: A (δ = 0.50 mm/s; ε = –0.03 mm/s; B_{hf} = 50.2 T) and B (δ = 0.40 mm/s; ε = –0.05 mm/s; B_{hf} = 47.1 T). We interpret the two sextets to be due to either differences in the coordination environment of iron, i.e., in tetrahedral or octahedral sites, the presence of a disordered surface phase, or a combination of both. We hope that provoking a discussion on the use of MBS for Fh will help develop a greater understanding of this mineral, and other short-range ordered iron minerals, which are so important in environmental processes.

Keywords: 2-line ferrihydrite, 6-line ferrihydrite, iron oxide, Mössbauer, fitting, parameters, hyperfine field

Introduction

Nanocrystalline Fe(III) oxyhydroxide mineral phases such as ferrihydrite (Fh) are ubiquitous in the environment and constitute a major component of the global bioavailable iron pool (Jambor and Dutrizac 1998). Many biogeochemical processes such as microbial Fe cycling directly involve Fh. For example, Fe(III)-reducing microorganisms can use Fh as a terminal electron acceptor, leading to the production of Fe(II), which further transforms Fh into other iron mineral phases such as goethite, magnetite, or siderite (Han et al. 2020; Hansel et al. 2003). On the other half of the Fe cycle, Fe(II)-oxidizing bacteria, which use Fe(II) as an electron donor, can precipitate Fh in soils and sediments (Kappler et al. 2021; Kappler and Straub 2005). Interactions between Fh and organic matter have also provoked much research, especially with regard to how organic matter-ferrihydrite (OM-Fh) complexes can undergo transformation to other mineral phases through reaction with Fe^{2+}_{aq}, protection of OM from degradation, and on the stabilization of Fh toward further transformation (ThomasArrigo et al. 2018; Zhou et al. 2018).

Despite its prevalence in nature, the structure of ferrihydrite remains a point of controversy, with several different models proposed. Fh is typically referred to as either being 2-line or 6-line based on the number of peaks observed when analyzed using X-ray diffraction (XRD). However, the Fh's nanoparticulate character and short-range-order mean that analysis of either type of Fh using (XRD) can be problematic (Cismasu et al. 2011). A study by Eggleton and Fitzpatrick suggested up to 36% Fe to be in tetrahedral coordination in Fh (Eggleton and Fitzpatrick 1988). This finding was followed up using ^{57}Fe Mössbauer spectroscopy (MBS) to investigate 6-line Fh at room temperature and concluded that the spectrum could be equally well fitted if Fh contained either 0 or 25% tetrahedral Fe (Cardile 1988). A study by Pankhurst and Pollard of both 2-line and 6-line Fh applied a magnetic field between 0–9 T and were able to see the clear splitting of the Fh spectra resulting in changes to the main hyperfine parameters isomer shift (δ), quadrupole shift (ε), and hyperfine magnetic field (B_{hf}), which indicated the presence of

* E-mail: james.byrne@bristol.ac.uk. Orcid 0000-0002-4399-7336

0003-004X/22/0008–1643$05.00/DOI: https://doi.org/10.2138/am-2021-7802

more than one Fe spectral component (Pankhurst and Pollard 1992). The authors determined these phases to be due to the existence of ferrimagnetism and antiferromagnetism for 2-line and 6-line Fh, respectively. Ultimately, the continued use of MBS to study Fh has not been able to conclusively prove or disprove the presence of tetrahedral Fe (Guyodo et al. 2006). Some of the more recent developments in understanding the structure of Fh have focused on the use of X-ray scattering to derive and model pair distribution function (PDF). Using this method, Michel et al. have argued for a structural model consisting of a unit cell with 12 Fe atoms in octahedral coordination and 1 Fe atom in tetrahedral coordination (Michel et al. 2010). This model is also supported by others who have used soft X-ray spectroscopy to study the crystal field environment of Fe in Fh (Peak and Regier 2012). In contrast, Drits et al. (1993) and Manceau (2011) have favored an entirely octahedrally coordinated Fe model, although the Michel et al. model appears to have gained the most widespread acceptance in recent years and several papers have further supported the presence of tetrahedral iron in Fh (Gilbert et al. 2013; Guyodo et al. 2012; Harrington et al. 2011; Maillot et al. 2011; Weatherill et al. 2016).

Outside of a description of iron's coordination number in Fh, the use of MBS appears to be rapidly growing in the study of Fh in environmental systems. One of the main strengths of MBS is its ability to distinguish Fe oxidation states in paramagnetic samples due to the distinctive hyperfine parameters corresponding to Fe(II) and Fe(III) phases, which typically have high- and low-isomer shift and quadrupole splitting values, respectively (Murad 2010). Furthermore, differences between the magnetic ordering temperature of different iron minerals provide the opportunity to characterize differences in the crystallinity in Fh coprecipitates in natural samples by a collection of spectra at different temperatures (Chen and Thompson 2021). The use of MBS for mineral identification can prove challenging as many non-unique solutions may exist, meaning that different analysts could come up with vastly different results if no predetermined criteria are agreed between them, with the identification of Fh being no exception. One of the most striking problems in establishing fitting routines for Fh is the fact that there is a frequent interchange between either a one, two, or sometimes three sextet approach. In well-established and often cited literature, such as Cornell and Schwertmann (2003), it is reported that only one sextet is needed for Fh when measured at liquid helium (LHe) temperature with hyperfine parameters (isomer shift [δ] = 0.24; quadrupole shift [ε] = –0.01; hyperfine magnetic field [B_{hf}] = 47) for 2-line and ($\delta = 0.25^{\#}$; $\varepsilon = -0.06$; $B_{hf} = 50$) for 6-line Fh [$^{\#}$note that the low-δ values reported indicates that the spectrometer was likely calibrated with something other than Fe(0)]. In contrast, an earlier study used two sextets to fit Fh with hyperfine parameters (Sextet 1: $\delta = 0.49$; $\varepsilon = -0.37$; $B_{hf} = 45.3$, Sextet 2: $\delta = 0.49$; $\varepsilon = 0.01$; $B_{hf} = 45.9$) (Murad 1988). These parameters diverge considerably from values reported in most other studies and might even suggest that the sample was incorrectly identified as Fh. This confusing situation of a differing number of sextets to use is not isolated, with many one sextet (Eusterhues et al. 2008) or two sextet (Pankhurst and Pollard 1992; Schwertmann et al. 2005) studies published. More recently, Dehouck et al. (2017) used a three-sextet approach to fit a range of samples used to simulate the potential transformation of ferrihydrite on the surface of Mars. In that study, a three-sextet fit provided the most satisfactory goodness of fit, but no interpretation of each site was suggested. In general, the absence of a standardized approach to fitting Fh or Fh-like Mössbauer spectra can lead to ambiguous interpretations, which could, in principle, lead to different spectroscopists reporting vastly different results even when given the same data set.

Coupled to this issue of how many sextets to use in the fitting is the selection of the model used to fit the data. A large range of software is available for Mössbauer analysis, however, almost all of them make use of similar approaches to fitting data, namely minimizing the difference between the model and the data by varying hyperfine parameters. Many of the models used for fitting environmental samples are based on a superposition of Lorentzian distribution to obtain good initial estimates of hyperfine parameters. However, natural samples, or samples with a distribution of individual hyperfine parameters, for instance, because of a distribution of particle sizes, are poorly fitted by this most basic approach. Alternatively, the Voigt (or pseudo-Voigt) profile (Prescher et al. 2012; Rancourt and Ping 1991), which is defined by a convolution between Lorentzian and Gaussian distributions, can be used to determine the probability distribution of one primary hyperfine parameter, which in the case of a sextet is the magnetic hyperfine field B_{hf}. Voigt fitting yields an additional parameter, which describes the standard deviation of the hyperfine field (σ_{Bhf}). In a further extension to the Voigt-based fitting approach, Lagarec and Rancourt (1997) later developed a method of obtaining the probability distribution of all three hyperfine sites δ, ε, and B_{hf}. This extended Voigt-based fitting provides more flexibility in terms of fitting spectra and is especially helpful for fitting environmental samples that are often comprised of a range of particle sizes. Using different models such as Lorentzian or Voigt can yield diverging results when fitting Fe minerals such as Fh, and so making an appropriate decision about which to use is critical to the success of the analysis. Furthermore, the higher number of fitting parameters available for more complex models such as xVBF can increase the likelihood of overinterpreting a spectrum. This is especially true for natural samples, which often contain multiple minerals (e.g., goethite, ferrihydrite, hematite, etc.) with overlapping features that are not easily constrained when the number of fitting parameters increases.

Here we present a study aimed at addressing the asymmetry of the Fh spectrum when measured at low temperature (Murad 1988), which has been often overlooked in the more recent literature, especially in environmental sciences. We place particular emphasis on addressing a largely ignored asymmetry of the Fh spectrum when measured at low temperature. This asymmetry cannot be explained by a one sextet fitting approach alone and provided the original motivation to investigate Fh in more detail. We present a comprehensive comparison of Fh Mössbauer data fitted using either one, two, or three sextets and compare the results obtained when using Lorentzian, Voigt, or extended Voigt based models. We also re-evaluate Fh produced by a marine Fe(II)-oxidizing bacteria and investigate how the hyperfine parameters of Fh change as a function of synthesis pH. Overall, we hope that this study will provide a more accurate approach to analyzing Fh in synthetic and natural samples.

Materials and methods

Mineral synthesis

Several different types of ferrihydrite were prepared for these experiments.

(1) 6-line Fh was synthesized by addition of $Fe(NO_3)_3 \cdot 9H_2O$ (20 g) into pre-heated (75 °C) deionized H_2O and rapidly stirred (Schwertmann and Cornell 2000). The solution was placed in an oven at 75 °C for 10 min and then rapidly cooled by plunging into ice water. The solution containing precipitate was then transferred into a dialysis bag and dialyzed for three days, replacing water several times per day. The final precipitate was then collected and freeze-dried.

(2) 2-line Fh was prepared by reaction of $Fe(NO_3)_3 \cdot 9H_2O$ (40 g) with KOH (1 M) until pH 7.0 (Schwertmann and Cornell 2000). The material was centrifuged (7500 rpm; 10 min) and washed in ultrapure H_2O (Milli-Q) to remove nitrate ions, with washing repeated three times. 2-line Fh was then freeze-dried.

(3) Biogenic Fh was prepared and analyzed by MBS during a published project by Swanner et al. (2015). In that study, a marine phototrophic Fe(II) oxidizer *Rhodovulum iodosum* produced short-range ordered Fe(III) (oxyhydr)oxide minerals, which were harvested after several days of incubation, and air-dried in an anoxic glovebox.

(4) pH-dependent Fh was prepared according to the approach of 2-line Fh (Schwertmann and Cornell 2000). However, samples were collected for analysis at various pH values (between pH 3–11) during the addition of KOH. Samples were not freeze dried and instead prepared for MBS by filtration (see below). Zeta potentials were measured at each corresponding pH value using a Zetasizer Nano ZSP (Malvern Instruments, U.K.).

^{57}Fe Mössbauer spectroscopy (MBS)

Freeze dried samples (2-line and 6-line Fh) were loaded as dried powers into Plexiglas holders (1 cm^2) and sealed inside an airtight bottle. Liquid suspended mineral precipitates (biogenic Fh and pH-dependent Fh) were passed through a filter (0.45 µm, mixed cellulose esters, Millipore) and then sealed between two layers of adhesive polyimide film (Kapton) and sealed in a Schott bottle. Samples were frozen at –20 °C while still in a N_2 atmosphere and stored for up to 1 month prior to loading into the instrument.

Each sample was inserted into a closed-cycle exchange gas cryostat (Janis cryogenics) with spectra measured either 295, 77, or 5 K using a constant acceleration drive system (WissEL) in transmission mode with a ^{57}Co/Rh source and calibrated against a 7 µm thick α-^{57}Fe foil measured at room temperature.

Spectra were analyzed using Recoil (University of Ottawa) by applying either the Lorentzian model, the Voigt Based Fitting (VBF) routine (Rancourt and Ping 1991), or the extended Voigt Based Fitting (xVBF) routine (Lagarec and Rancourt 1997). The main difference between VBF and xVBF fitting routines is the ability for the latter to include a distribution of the hyperfine parameters δ, ε, and B_{hf} [denoted σ(δ), σ(ε), σ(B_{hf}), respectively]. In contrast, the VBF fitting routine only permits a distribution of B_{hf} [σ(B_{hf})]. The half-width at half maximum (HWHM) was fixed to a value of 0.125 mm/s for all samples, which was determined to be the inner line broadening of the calibration foil at room temperature. Online Materials[1] Table S1 denotes the parameters that were unconstrained and constrained during fitting. Recoil offers the possibility of adding more than one component per sextet, having equal isomer shifts and quadrupole shifts but with a distribution of hyperfine fields. We applied multi-component fitting for 2-line Fh with the xVBF model as described below (Online Materials[1] Fig. S2). For the raw data set, see Byrne and Kappler (2022).

Results

2-line and 6-line Fh

The raw data without fits for the MBS for 2-line and 6-line Fh collected at 295, 77, and 5 K are shown in Figure 1. At 295 K, both samples exhibit superparamagnetic behavior as indicated by the clear dominance of a doublet, with no evidence for a sextet. Some asymmetry is notable in the 6-line Fh sample, with the left peak of the doublet having lower intensity than the right peak. The spectra show that 2-line Fh remained superparamagnetic until below 77 K as indicated by the absence of a clear sextet. In comparison, 6-line Fh was already undergoing magnetic ordering above 77 K, as indicated by the presence of a partially ordered sextet at 77 K. At 5 K, the asymmetry of both 2-line and 6-line

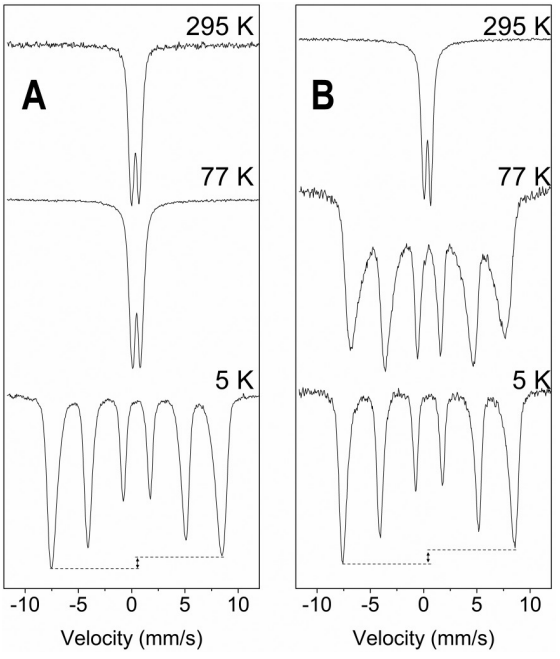

Figure 1. ^{57}Fe Mössbauer data collected for (**a**) 2-line Fh and (**b**) 6-line Fh at 295, 77, and 5 K. The dashed line shown for the 5 K spectra indicates the asymmetry, which is observable when measured at liquid helium temperature.

Fh is slight but obvious, with the first and six lines of each sextet having a clear difference in intensity. The magnitude of the asymmetry (α) is calculated according to Equation 1.

$$\alpha(\%) = \Delta_6/\Delta_1 \times 100 \quad (1)$$

where Δ_1 and Δ_6 correspond to the difference between the baseline and maximum amplitude of peaks 1 and 6, respectively. The asymmetry parameter is calculated as 7.4 and 10.6% for 2-line and 6-line FH, respectively. These values of α represent clear evidence that the spectra do not obey the symmetrical line intensities (i.e., 3:2:1:1:2:3) expected of single magnetic sublattice such as a pure powdered mineral phase (Murad 2013).

Further evidence of the asymmetry in 2-line and 6-line spectra collected at 5 K is shown in Figure 2. The figure shows the results from fitting both spectra with between one and three sextets with the Lorentzian, Voigt, and extended Voigt models available in Recoil (Lagarec and Rancourt 1998). With only a one sextet fit, each model provides almost identical δ, ε, and B_{hf} for both 2-line and 6-line Fh (Table 1).

In the two-site approach, the site with a larger hyperfine magnetic field is denoted A (average B_{hf} = 50.2 T for all models), whereas the sextet with a narrower hyperfine magnetic field is denoted B (average B_{hf} = 47.5 T for all models). With the two-sextet approach, clearer differences between 2-line and 6-line Fh begin to emerge, specifically in the relative abundances of each sextet. The 2-line Fh B site sextets have spectral areas of 46.5 ±1.1%, 52.9 ±0.6%, and 45.2 ±4.1% for Lorentzian, VBF, and xVBF modeling approaches, respectively. In comparison, the 6-line B sextets have spectral areas

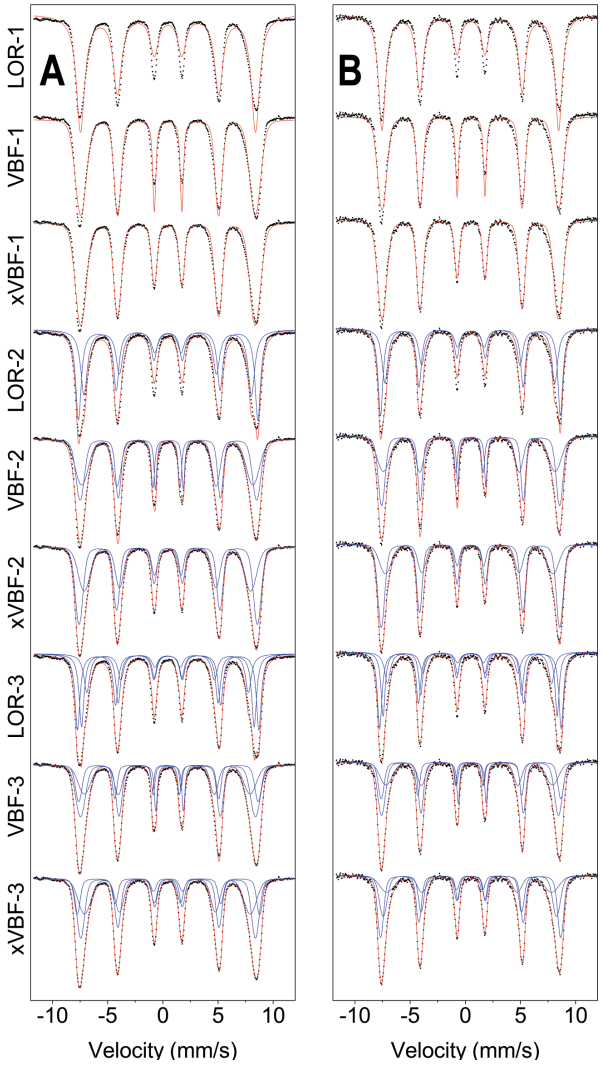

Figure 2. Fitting results for (**a**) 2-line and (**b**) 6-line FH. Data shown were fit with Lorentzian line (LOR), Voigt (VBF), and extended Voigt models (xVBF). Numbers after each label refer to one, two, or three sextet fits, respectively. (Color online.)

of 43.2 ± 2.5%, 46.6 ± 1.6%, and 36.5 ± 4.4% for Lorentzian, VBF, and xVBF modeling approaches, respectively. As sextet B has the lowest hyperfine field, we suggest that it could correspond to a different magnetic sublattice with different Fe-O-Fe distances or to a more disordered phase than sextet A (see discussion). Based on visual inspection, even though the asymmetry has been addressed, the Lorentzian model is only able to fit the data poorly with the xVBF model (that enables the fitting of probability distributions for δ, ε, and B_{hf} compared to VBF model, which only fits a probability distribution for B_{hf}) providing the most satisfactory fit.

The three-sextet approach is more complex with an additional sextet C required, which has the lowest hyperfine magnetic field of all sextets with average B_{hf} = 46.3 T. The relative area of this third sextet ranges from 23.1 ± 2.3% to 38.7 ± 8.6%, indicating a wide range of potential solutions. Furthermore, the C sextets all have larger $\sigma(B_{hf})$ compared to either the A or B sextets (Table 1).

Figure 3 shows a comparison of residuals (i.e., the difference between data and model) as well as the goodness of fit (reduced χ^2) for each model used. The goodness of fit is not necessarily the best measure of fitting accuracy as it is influenced by the signal-to-noise ratio. For instance, if the signal-to-noise ratio is high with an almost flat background region, reduced χ^2 is likely to be much higher than if the exact same sample was measured at a lower concentration and had a poorer signal-to-noise ratio. However, reduced χ^2 can still provide a rule of thumb for how well the model fits the data, and in general, spectral fits with reduced $\chi^2 \leq 1$ are considered to provide a good representation of the data. The residuals shown in Figure 3a confirm the expectations from visual inspection of the data shown in Figure 2 that a one sextet approach to fitting is unable to accurately describe the data with several peaks and troughs that are characteristic of an insufficiently fitted spectrum. These peaks and troughs are visible for all models apart from xVBF fitted with either two or three sextets.

Figure 3b shows a comparison between the goodness of fits for all fitted spectra. The reduced χ^2 is above 5 for every 2-line Fh model fitted with only one sextet. 6-line Fh has reduced χ^2 above 5 for all one sextet models except the xVBF model, which has reduced χ^2 = 4.7. As the number of sextets used for fitting increases, reduced χ^2 decreases. However, the xVBF model consistently provides the best results, though this is also due to the fact that there are more parameters available to vary than in the other fitting models.

To evaluate if a single sextet, multi-component fit would yield a better agreement with the data we also fitted 2-line Fh data using the xVBF model with a single sextet and increasing number of hyperfine field components. This enabled a non-Gaussian distribution of B_{hf} and is often used during fitting samples with non-homogenous size distributions (Online Materials[1] Fig. S2). Increasing the number of components led to a decrease in the amplitude of the peaks and troughs in the residual, indicating an improvement in the fit. However, the hyperfine parameter histograms (Online Materials[1] Fig. S2u–S2y) show deviations from a symmetric or even skewed profile. When 1 sextet and 3 components are used, the histogram has two peaks. Furthermore, closer inspection of peak 1 (Online Materials[1] Fig. S2h) and peak 6 (Online Materials[1] Fig. S2m) suggest that the fit does not match up well with the data. In contrast, fitting with 2 or 3 sextets and only 1 component (Online Materials[1] Figs. S2d and S2e) show close agreement between the data and fit, residuals with little pattern, and clear probability distributions.

Biogenic Fh

To evaluate if the asymmetry was confined to chemically synthesized, freeze-dried Fh, we re-evaluated data measured for biogenic Fh from a marine phototrophic Fe(II)-oxidizing bacterium, *Rhodovulum iodosum*, which was collected for a study published in 2015 (Swanner et al. 2015) (Fig. 4). This data was originally fit with one xVBF sextet with δ = 0.49 mm/s, ε = –0.06 mm/s, B_{hf} = 49.4 T, reduced χ^2 = 1.4. While this original fitting provided a reasonable assessment of the data with an

TABLE 1. Hyperfine parameters obtained for fitting 2-line and 6-line Fh with Lorentzian (LOR), Voigt (VBF), or extended Voigt (xVBF) models

Model	Sample	N_{sx}	Sextet	δ mm/s	±	σ(δ) mm/s	ε mm/s	±	σ(ε) mm/s	B_{hf} *T*	±	σ(B_{hf}) *T*	±	w mm/s	±	R.A. %	±	Red. χ^2
LOR	2L	1	A	0.468	0.001		−0.004	0.001		49.20	0.01	–	–	0.45	0.00	100.0		66.34
LOR	6L	1	A	0.484	0.003		−0.032	0.003		49.68	0.02	–	–	0.38	0.00	100.0		11.78
VBF	2L	1	A	0.468	0.001		−0.005	0.001		49.04	0.01	2.79	0.01	–	–	100.0		39.84
VBF	6L	1	A	0.483	0.002		−0.034	0.002		49.56	0.02	2.26	0.03	–	–	100.0		7.55
xVBF	2L	1	A	0.467	0.001	0.128	−0.004	0.001	0.128	49.04	0.01	2.51	0.02	–	–	100.0		16.64
xVBF	6L	1	A	0.482	0.002	0.101	−0.033	0.002	0.101	49.57	0.02	2.03	0.03	–	–	100.0		4.65
LOR	2L	2	A	0.479	0.002		−0.002	0.002		50.43	0.02	–	–	0.30	0.00	53.5	1.0	24.87
LOR	2L	2	B	0.447	0.002		−0.008	0.002		47.08	0.30	–	–	0.36	0.01	46.5	1.1	
LOR	6L	2	A	0.493	0.003		−0.030	0.003		50.58	0.03	–	–	0.27	0.01	56.8	2.4	5.06
LOR	6L	2	B	0.456	0.005		−0.045	0.005		47.78	0.07	–	–	0.32	0.01	43.2	2.5	
VBF	2L	2	A	0.544	0.003		−0.043	0.003		49.63	0.02	2.06	0.03	–	–	47.1	0.6	12.98
VBF	2L	2	B	0.361	0.004		0.037	0.004		48.13	0.04	3.43	0.04	–	–	52.9	0.6	
VBF	6L	2	A	0.532	0.004		−0.052	0.004		50.04	0.04	1.60	0.05	–	–	53.4	1.6	2.66
VBF	6L	2	B	0.366	0.010		−0.009	0.008		48.28	0.12	3.27	0.10	–	–	46.6	1.6	
xVBF	2L	2	A	0.487	0.005	0.124	−0.003	0.002	0.124	50.11	0.04	1.51	0.07	–	–	54.8	4.1	3.20
xVBF	2L	2	B	0.424	0.004	0.133	−0.012	0.003	0.133	46.81	0.39	2.79	0.17	–	–	45.2	4.1	
xVBF	6L	2	A	0.500	0.006	0.099	−0.032	0.003	0.099	50.18	0.04	1.35	0.08	–	–	63.5	4.4	1.14
xVBF	6L	2	B	0.405	0.011	0.103	−0.055	0.010	0.103	47.11	0.51	2.90	0.25	–	–	36.5	4.4	
LOR	2L	3	A	0.478	0.002		0.003	0.002		50.99	0.03	–	–	0.27	0.00	39.2	1.2	11.84
LOR	2L	3	B	0.466	0.002		−0.013	0.002		48.52	0.03	–	–	0.26	0.01	37.0	1.7	
LOR	2L	3	C	0.426	0.004		−0.003	0.040		45.42	0.05	–	–	0.32	0.01	23.7	1.1	
LOR	6L	3	A	0.491	0.004		−0.025	0.004		51.02	0.05	–	–	0.24	0.01	43.7	2.8	2.60
LOR	6L	3	B	0.480	0.004		−0.045	0.004		48.95	0.05	–	–	0.22	0.01	33.2	3.8	
LOR	6L	3	C	0.422	0.010		−0.041	0.010		46.15	0.12	–	–	0.31	0.02	23.1	2.3	
VBF	2L	3	A	0.431	0.005		0.074	0.005		50.46	0.05	1.53	0.08	–	–	22.9	2.0	5.73
VBF	2L	3	B	0.535	0.005		−0.075	0.005		49.18	0.04	2.42	0.03	–	–	45.2	1.7	
VBF	2L	3	C	0.354	0.007		0.043	0.006		46.61	0.30	3.22	0.15	–	–	31.8	2.0	
VBF	6L	3	A	0.460	0.010		0.057	0.012		50.52	0.09	1.32	0.13	–	–	24.8	3.6	1.28
VBF	6L	3	B	0.523	0.010		−0.100	0.011		49.75	0.07	1.85	0.07	–	–	45.4	3.3	
VBF	6L	3	C	0.373	0.014		−0.014	0.012		46.78	0.57	3.18	0.20	–	–	29.8	3.8	
xVBF	2L	3	A	0.481	0.008	0.127	0.020	0.021	0.127	51.28	0.18	0.55	0.42	–	–	19.0	11.0	2.33
xVBF	2L	3	B	0.490	0.006	0.121	−0.018	0.005	0.121	49.11	0.55	1.51	0.36	–	–	42.0	11.0	
xVBF	2L	3	C	0.409	0.008	0.131	0.000	0.005	0.131	46.59	0.40	3.07	0.15	–	–	38.7	8.6	
xVBF	6L	3	A	0.501	0.009	0.111	−0.018	0.025	0.111	50.65	0.15	0.94	0.37	–	–	42.0	18.0	0.86
xVBF	6L	3	B	0.481	0.012	0.074	−0.066	0.013	0.074	48.74	1.20	1.74	0.60	–	–	34.0	20.0	
xVBF	6L	3	C	0.373	0.027	0.098	−0.014	0.022	0.098	46.28	0.82	3.65	0.38	–	–	24.0	10.0	

Notes: N_{sx} = Number of sextets per model; Sextet = Indicates each sextet; δ = isomer shift (mm/s); σ(δ) = standard deviation of the isomer shift; ε = quadrupole shift (mm/s); σ(ε) = standard deviation of the quadrupole shift; B_{hf} = hyperfine magnetic field (T); σ(B_{hf}) = standard deviation of hyperfine magnetic field (T); w = linewidth of the Lorentzian (mm/s), R.A. = relative abundance (%); Red. (reduced) χ^2 = goodness of fit.

acceptable goodness of fit, a closer evaluation of the raw data reveals some asymmetry (α = 4.9%), and the residual reveals peaks and troughs similar to either 2-line or 6-line Fh (Fig. 3a) when fitted with just one sextet, though not as intense. When the spectrum was re-evaluated with two xVBF sextets, the asymmetry was no longer visible, and the residual showed a more uniform pattern (Online Materials[1] Table S1; reduced $\chi^2 = 0.6$). The hyperfine parameters for sextet A were $\delta = 0.50 \pm 0.01$ mm/s, $\varepsilon = -0.07 \pm 0.01$ mm/s, $B_{hf} = 49.9 \pm 0.08$ T, R.A. = 57 ± 6%, with sextet B having $\delta = 0.45 \pm 0.03$ mm/s, $\varepsilon = -0.04 \pm 0.02$ mm/s, $B_{hf} = 47.0 \pm 0.7$ T, R.A. = 43 ± 6% both of which were consistent with results obtained for 2-line and 6-line Fh when fitted with two sextets and the xVBF model. Comparing these hyperfine parameters with those determined for synthetic Fh it is difficult to determine if the biogenic sample is closer to 2-line or to 6-line Fh and so is best described as simply biogenic Fh (Online Materials[1] Fig. S3). Even though the differences between the hyperfine parameters appear relatively minor, a better understanding of the accurate structure of Fh can help to explain its importance in biogeochemical systems such as these.

Analysis of Fh synthesized at different pH

We performed an additional experiment to evaluate Fh using MBS focused on the formation of Fe(III)-precipitates using the standard protocol used to synthesize Fh, but with samples collected at different pH (Online Materials[1] Fig. S1; Online Materials[1] Table S1). These samples were collected during the precipitation of 2-line Fh and then subsequently analyzed at 5 K. Figure 5 shows a comparison between different hyperfine parameters as a function of Fh synthesis-pH obtained by fitting each spectrum with two xVBF sextets. The data show a clear distinction between the two sextets at all pH. The isomer shift exhibits a linear correlation with synthesis-pH, with sextet B showing a stronger negative linear correlation than sextet A, suggesting that the effect of pH was more strongly associated with the B sextet. The magnetic hyperfine field of both sites appears to increase as a function of pH. The quadrupole shift shows some positive correlation to the Fh synthesis pH. Finally, the relative abundance of sextet A and sextet B appears to change as a function of pH, with the A and B sextets occupying a decreasing and increasing proportion of the spectral area, respectively, as synthesis pH increases.

These data indicate that the properties of Fh change as a function of synthesis pH, which, as far as we are aware, has not been previously shown by MBS. Potentially, these differences might also reflect a change in the Fh surface properties, for example, ζ potential (ZP), which was also measured for these samples. Changes to the ζ potential occur as a result of a change in the surface charge of the ferrihydrite, which is positive below the point of zero charge (PZC) and negative above (Li et al. 2015).

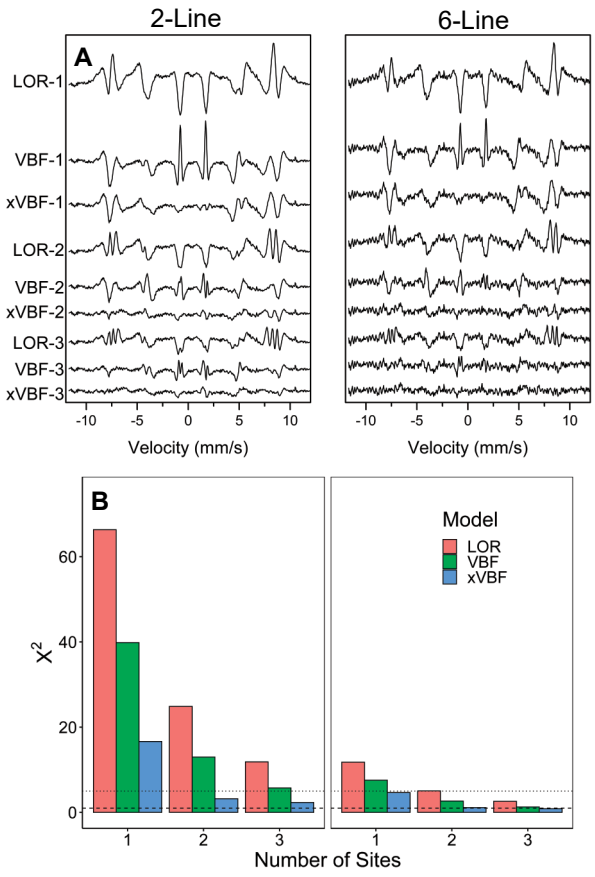

Figure 3. Comparison of fitting quality. (**a**) Residuals indicating the difference between data and fit of 2-line and 6-line ferrihydrite. (**b**) Reduced χ^2 of all fitting approaches for 2-line and 6-line Fh. Dashed line represents reduced $\chi^2 = 1$, with dotted line indicating reduced $\chi^2 = 5$. (Color online.)

Figure 6 shows a side-by-side comparison of changes in ZP, δ (Sextet A), δ (Sextet B) as a function of pH (both y-axes for δ span a range of 0.025 mm/s). Interestingly, the δ of both A and B sextets appear to change just before the point of zero charge (PZC; pH = 8.3), with the B sextet exhibiting the largest change. The changes are relatively small, however, this provides support to the idea that the B sextet corresponds to a surface-bound site.

Discussion

When fitting Mössbauer data, it is best practice to find an appropriate fit with an acceptable reduced χ^2 using the least number of sextets or doublets. This is necessary to prevent "over fitting", which can lead to a poor interpretation of the sample (Hargraves et al. 1990). In the 2-line and 6-line Fh spectra (Figs. 1 to 3; Table 1), the smallest reduced χ^2 was consistently achieved when using the xVBF model. This is particularly evident from inspection of the residuals though smaller reduced χ^2 is likely to be also due to a higher number of parameters available for xVBF compared to the Lorentzian or VBF fitting approaches. The issue of asymmetry was resolved by fitting with two sextets for 2-line and 6-line Fh with reduced $\chi^2 = 3.2$ and reduced $\chi^2 = 1.14$, respectively. Reduced χ^2 remained above 1 for 2-line Fh (reduced $\chi^2 = 2.4$) even when a three sextet xVBF model was used. 6-line Fh had reduced $\chi^2 = 0.86$ when fitted with a three sextet xVBF model. Even though a three-sextet approach provides the best fit, the correct assignment of each site becomes more and more complex. We suggest that the two-sextet approach is the safest option and still allows the physical interpretation of each site.

In order for the two-sextet approach to be accepted, a better understanding of each site needs to be considered. We hypothesize that a two-sextet model can be explained by either: (I) coordination of iron atoms in tetrahedral and octahedral sites, (II) surface disorder, or (III) a combination of the two.

(I) Tetrahedral and octahedral sites

The structure of ferrihydrite remains under debate, with several different models proposed for its structure. Eggleton and Fitzpatrick suggest up to 36% Fe to be in tetrahedral coordination in Fh (Eggleton and Fitzpatrick 1988). Peak and Regier (2012) suggested as much as 30–40% tetrahedral iron, which was in close agreement with other X-ray spectroscopic results (Guyodo et al. 2012; Maillot et al. 2011). Michel et al. (2007) argued for an ideal structure, which contained 20% tetrahedral Fe, but that vacancies may mean that some tetrahedral sites are empty, lead-

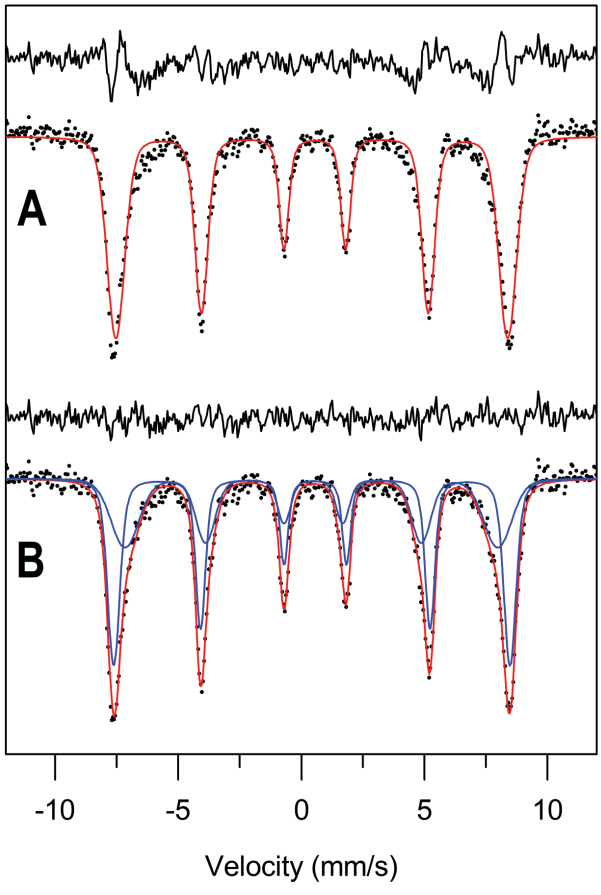

Figure 4. Biogenic ferrihydrite fitted with 1 sextet (**a**) compared with 2 sextets (**b**) with the xVBF fitting routine. Black lines indicate the residual, i.e., difference between model and data. Data from Swanner et al. (2015) reproduced with permission (Copyright 2015 Elsevier Ltd). (Color online.)

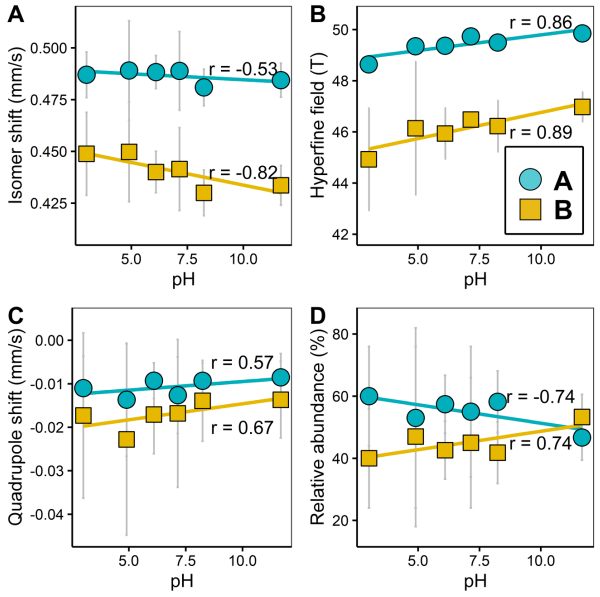

Figure 5. Hyperfine parameters of Fh synthesized at different pH fitted with two xVBF sextets. Turquoise lines correspond to sextet A, yellow lines to sextet B. Error bars indicate uncertainty for each parameter provided by the fitting software. (Color online.)

ing to a unit cell with 12 Fe atoms in octahedral coordination and 1 Fe atom in tetrahedral coordination (i.e., 7.7% tetrahedral Fe) (Michel et al. 2010). Previous studies have separated tetrahedral and octahedral coordinated iron on the basis of isomer shift in MBS spectra, with lower δ being more indicative of tetrahedral iron (Cuadros et al. 2019; Kuzmann et al. 2003). The average δ for the A and B sextets shown when fitted with 2 sextets (Table 1) were 0.503 ± 0.036 mm/s and 0.410 ± 0.045 mm/s for 2-line Fh, respectively. For 6-line Fh, A and B sextets had δ of 0.508 ± 0.021 mm/s and 0.409 ± 0.045 mm/s, respectively (average is based on all models with errors calculated as the standard deviation from the mean). This would suggest that the B site could correspond to tetrahedral iron in ferrihydrite. However, the attempt to detect tetrahedral Fe(III) in Fh by Mössbauer is not new and faces several obstacles. As already outlined in the introduction section, the use of Mössbauer for the identification of tetrahedral and octahedral sites has been previously rejected. Because tetrahedral Fe contents are frequently low, the uncertainty associated with the correspondingly low-intensity peaks in the Mössbauer spectra is high. Furthermore, there is overlap between the low-energy lines (low-velocity values) of tetrahedral Fe(III) and octahedral Fe(III) (Coey et al. 1984; Rancourt et al. 1992), making it difficult to identify tetrahedral Fe(III) and quantify it. However, considering our data and assuming the Eggleton and Fitzpartick model in which 36% of the Fe in 6-line Fh is in tetrahedral coordination, this would line up precisely with our reported values for the B sextet when fitted with a two sextet xVBF model (Table 1). Considering our observation that the isomer shift of sextet B varies with pH (Fig. 6), that would raise the question of how pH influences tetrahedral Fe(III)? Alternatively, if we assume the Michel model to be correct, then this would imply ~8% of the Fe is tetrahedrally coordinated. Looking at the two-sextet model, the relative abundance of A vs. B sextets far exceed this value, and it is unlikely that such a minor component would be discernible in the spectra. Even in the three sextet xVBF model, the relative abundances of A, B, and C sextets are much greater than this value. These conflicting structural interpretations of Fh mean that we cannot explain the asymmetry as being due to the presence of tetrahedral iron within the 2-line and 6-line Fh.

(II) Surface disorder

The effect of surface disorder in ultrafine nanoparticles has been considered for iron (oxyhydr)oxides (Dormann et al. 1999; Mørup 1990; Tronc et al. 2000) and is potentially important in Fh (Hiemstra 2013). Typically, the primary particles of 2-line Fh are estimated to have a size of ca. 3 nm, compared to 6-line Fh, which has an average diameter of 2–6 nm (Schwertmann and Cornell 2000). We did not independently verify the particle size of the Fh in this study but consider the reliability of the synthesis procedures to be satisfactory for this discussion. It was estimated by Zhao et al. (1994) that assuming a spherical shape, ferrihydrite has a surface shell with a thickness of ~2 Å (equivalent to one Fe^{3+}-O bond distance). Based on estimated particle sizes (taking $d = 3$ nm and $d = 4$ nm for 2-line and 6-line Fh, respectively), this would correspond to 35 and 27% of the

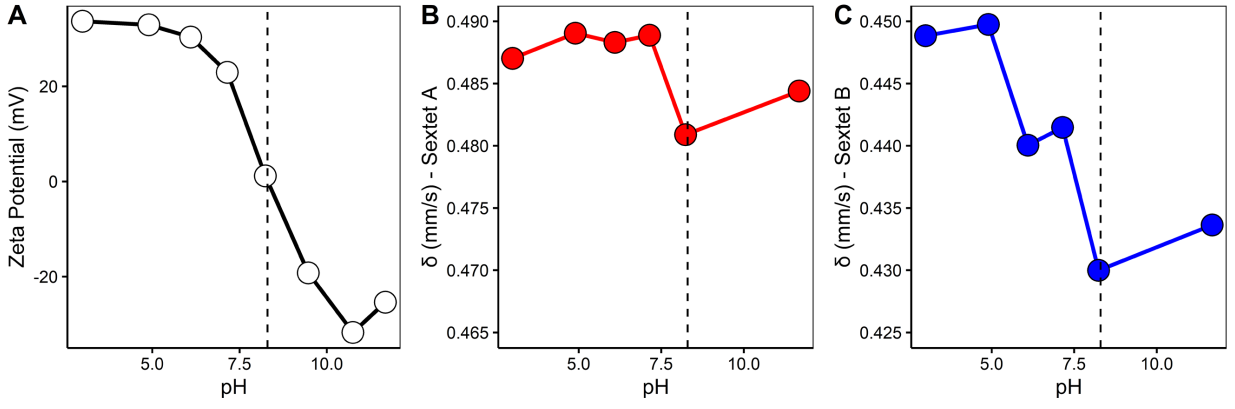

Figure 6. Changes to Fh (**a**) ζ potential (ZP), (**b**) isomer shift of sextet A, and (**c**) isomer shift of sextet B as a function of synthesis pH (both y-axes for δ span a range of 0.025 mm/s). Dashed line indicates point of zero charge (pH = 8.3). (Color online.)

total particle for 2-line and 6-line Fh, respectively (Zhao et al. 1994). These values show reasonable comparison to the relative areas of the B sites when fitted with two xVBF sextets, which were 45.2 and 36.5% for 2-line and 6-line Fh, respectively. The effect of surface disorder was previously discussed by (Hiemstra 2013) who suggested that the mineral core of Fh is defect free and that the size-dependent variation is surface driven. This hypothesis is analogous to our observed pH-dependent measurements in which the largest changes to the isomer shift were observed for the B sextet, which we tentatively assume could correspond to the surface sites, especially as these changes line up with changes to the ZP.

(III) Combination of the above

We must also consider the possibility that the asymmetry frequently observed in ferrihydrite when measured at liquid helium temperature is due to both a combination of tetrahedral Fe and the effect of surface disorder. This would then be best fitted using a four-sextet fit to account for tetrahedral and octahedral iron in both the surface and the bulk. However, if we were to consider a hypothetical Fh particle with 35% Fe atoms located at the surface and 65% Fe atoms located in the core, any tetrahedral sextets would account for 3 and 5.4% of the spectral area in surface and core sites, respectively (according to the Michel model). Such minor components would be difficult to distinguish against the background, and it is unlikely that the mathematical fitting models used to fit the data would be able to provide accurate results. In fact, a four-sextet fit was tested using the xVBF model and was unable to provide any reasonable improvement to the two or three sextet fits (data not shown).

Alternative explanations for a multi sextet Fh model other than those suggested above cannot be entirely ruled out. For example, a recent study considered whether 2-line Fh was a multi-phase nanocomposite consisting of ordered nanodomains embedded in a short-range ordered ferric hydroxide matrix (Funnell et al. 2020). Another study considered the distribution of structure types in such a nanocomposite to depend on particle size, temperature, and hydration (Sassi et al. 2021). The Mössbauer spectrum of such a system could conceivably require a two-sextet fit, but it is unclear how different such a spectrum might look from those reported in this study and warrants further consideration.

Implications

The interpretation of the two-sextet model for Fh remains open for debate and we do not consider that Mössbauer can provide a definitive answer. However, it is likely that there is at least some surface disorder, which should be accounted for that potentially influences tetrahedral iron. These results have clear implications for a wide range of studies. For example, the understanding of iron transformation in laboratory or environmental systems frequently rely on the accurate identification of Fh. In many cases, these phases are associated with other minerals such as goethite, lepidocrocite, magnetite, Fe-sulfides, and phyllosilicates. Quick identification of Fh commonly relies on the observation of a single sextet with hyperfine parameters such as those previously reported (Cornell and Schwertmann 2003). Our two-sextet model adds to the complexity of determining the mineral phase present in a natural sample. For example, if the amount of ferrihydrite in a sample is low in comparison to another mineral, which is also magnetically ordered and shares similar hyperfine parameters (e.g., goethite), then the application of two sextets for fitting ferrihydrite could lead to ambiguities in the outcome of the fit (Chen and Thompson 2021). In such cases, we would suggest maintaining the single sextet approach, which now acts as more of an average solution to Fh. Further to this, however, samples should also be measured at several other temperatures to ease interpretation. These results also have implications on the potential complexation of Fh with organic matter (OM). It might be anticipated that any sorption of OM to Fh will be dependent on the surface of the mineral. Therefore, we anticipate that the biggest changes to the Fh structure will occur to the B sextet.

In summary, we recommend the most appropriate model for fitting either 2-line or 6-line ferrihydrite at liquid helium temperature is the xVBF model, with two sextets:

2-lineFh: A [δ = 0.49 mm/s; ε = 0.00 mm/s; B_{hf} = 50.1 T; $\sigma(B_{hf})$ = 1.51] and B [δ = 0.42 mm/s; ε = –0.01 mm/s; B_{hf} = 46.8 T; $\sigma(B_{hf})$ = 2.79]
6-line Fh: A [δ = 0.50 mm/s; ε = –0.03 mm/s; B_{hf} = 50.2 T; $\sigma(B_{hf})$ = 1.35] and B [δ = 0.40 mm/s; ε = –0.05 mm/s; B_{hf} = 47.1 T; $\sigma(B_{hf})$ = 2.90].

Acknowledgments and Funding

Timm Bayer is thanked for preparation of pH-dependent Fh. Ying Ji and Susan Tandy are thanked for providing 2-line and 6-line FH. Aaron Thompson (University of Georgia), Elizabeth Sklute (Mount Holyoke College), and other anonymous reviewers are thanked for providing critical feedback, which has helped to improve the quality of the manuscript. A.K. acknowledges the infrastructural support by the DFG under Germany's Excellence Strategy, cluster of Excellence EXC2124, project ID 390838134. Raw data from this manuscript is available for download from IEDA (see Byrne and Kappler 2022).

References cited

Byrne, J., and Kappler, A. (2022) A revised analysis of ferrihydrite at liquid helium temperature using Mössbauer spectroscopy, Version 1.0. Interdisciplinary Earth Data Alliance (IEDA). https://doi.org/10.26022/IEDA/112329. Accessed 2022-06-21.

Cardile, C. (1988) Tetrahedral Fe^{3+} in ferrihydrite: ^{57}Fe Mössbauer spectroscopic evidence. Clays and Clay Minerals, 36, 537–539.

Chen, C., and Thompson, A. (2021) The influence of native soil organic matter and minerals on ferrous iron oxidation. Geochimica et Cosmochimica Acta, 292, 254–270.

Cismasu, A.C., Michel, F.M., Tcaciuc, A.P., Tyliszczak, T., and Brown, G.E. Jr. (2011) Composition and structural aspects of naturally occurring ferrihydrite. Comptes Rendus Geoscience, 343, 210–218.

Coey, J.M.D., Chukhrov, F.V., and Zvyagin, B.B. (1984) Cation distribution, Mössbauer spectra, and magnetic properties of ferripyrophyllite. Clays and Clay Minerals, 32, 198–204.

Cornell, R.M., and Schwertmann, U. (2003) The Iron Oxides Structure, Properties, Reactions, Occurrences and Uses. Wiley-VCH.

Cuadros, J., Michalski, J.R., Dyar, M.D., and Dekov, V. (2019) Controls on tetrahedral Fe(III) abundance in 2:1 phyllosilicates. American Mineralogist, 104, 1608–1619.

Dehouck, E., McLennan, S.M., Sklute, E.C., and Dyar, M.D. (2017) Stability and fate of ferrihydrite during episodes of water/rock interactions on early Mars: An experimental approach. Journal of Geophysical Research: Planets, 122, 358–382.

Dormann, J., Fiorani, D., Cherkaoui, R., Tronc, E., Lucari, F., d'Orazio, F., Spinu, L., Nogues, M., Kachkachi, H., and Jolivet, J. (1999) From pure superparamagnetism to glass collective state in γ-Fe_2O_3 nanoparticle assemblies. Journal of Magnetism and Magnetic Materials, 203, 23–27.

Drits, V., Sakharov, B., Salyn, A., and Manceau, A. (1993) Structural model for ferrihydrite. Clay Minerals, 28, 185–207.

Eggleton, R.A., and Fitzpatrick, R.W. (1988) New data and a revised structural model for ferrihydrite. Clays and Clay Minerals, 36, 111–124.

Eusterhues, K., Wagner, F.E., Häusler, W., Hanzlik, M., Knicker, H., Totsche, K.U.,

Kögel-Knabner, I., and Schwertmann, U. (2008) Characterization of ferrihydrite-soil organic matter coprecipitates by X-ray diffraction and Mössbauer spectroscopy. Environmental Science & Technology, 42, 7891–7897.
Funnell, N.P., Fulford, M.F., Inoué, S., Kletetschka, K., Michel, F.M., and Goodwin, A.L. (2020) Nanocomposite structure of two-line ferrihydrite powder from total scattering. Communications Chemistry, 3, 1–9.
Gilbert, B., Erbs, J.J., Penn, R.L., Petkov, V., Spagnoli, D., and Waychunas, G.A. (2013) A disordered nanoparticle model for 6-line ferrihydrite. American Mineralogist, 98, 1465–1476.
Guyodo, Y., Banerjee, S.K., Lee Penn, R., Burleson, D., Berquo, T.S., Seda, T., and Solheid, P. (2006) Magnetic properties of synthetic six-line ferrihydrite nanoparticles. Physics of the Earth and Planetary Interiors, 154, 222–233.
Guyodo, Y., Sainctavit, P., Arrio, M.-A., Carvallo, C., Lee Penn, R., Erbs, J.J., Forsberg, B.S., Morin, G., Maillot, F., Lagroix, F., Bonville, P., Wilhelm, F., and Rogalev, A. (2012) X-ray magnetic circular dichroïsm provides strong evidence for tetrahedral iron in ferrihydrite. Geochemistry, Geophysics, Geosystems, 13.
Han, X., Tomaszewski, E.J., Sorwat, J., Pan, Y., Kappler, A., and Byrne, J.M. (2020) Effect of microbial biomass and humic acids on abiotic and biotic magnetite formation. Environmental Science & Technology, 54, 4121–4130.
Hansel, C.M., Benner, S.G., Neiss, J., Dohnalkova, A., Kukkadapu, R.K., and Fendorf, S. (2003) Secondary mineralization pathways induced by dissimilatory iron reduction of ferrihydrite under advective flow. Geochimica et Cosmochimica Acta, 67, 2977–2992.
Hargraves, P., Rancourt, D.G., and Lalonde, E. (1990) Single-crystal Mössbauer study of phlogopite mica. Canadian Journal of Physics, 68, 128–144.
Harrington, R., Hausner, D.B., Xu, W., Bhandari, N., Michel, F.M., Brown, G.E., Jr, Strongin, D.R., and Parise, J.B. (2011) Neutron pair distribution function study of two-line ferrihydrite. Environmental Science & Technology, 45, 9883–9890.
Hiemstra, T. (2013) Surface and mineral structure of ferrihydrite. Geochimica et Cosmochimica Acta, 105, 316–325.
Jambor, J.L., and Dutrizac, J.E. (1998) Occurrence and constitution of natural and synthetic ferrihydrite, a widespread iron oxyhydroxide. Chemical Reviews, 98, 2549–2586.
Kappler, A., Bryce, C., Mansor, M., Lueder, U., Byrne, J.M., and Swanner, E.D. (2021) An evolving view on biogeochemical cycling of iron. Nature Reviews. Microbiology, 19, 360–374.
Kappler, A., and Straub, K.L. (2005) Geomicrobiological cycling of iron. Reviews in Mineralogy and Geochemistry, 59, 85–108.
Kuzmann, E., Nagy, S., and Vértes, A. (2003) Critical review of analytical applications of Mössbauer spectroscopy illustrated by mineralogical and geological examples (IUPAC Technical Report). Pure and Applied Chemistry, 75, 801–858.
Lagarec, K., and Rancourt, D.G. (1997) Extended Voigt-based analytic lineshape method for determining N-dimensional correlated hyperfine parameter distributions in Mössbauer spectroscopy. Nuclear Instruments and Methods in Physics Research Section B: Beam Interactions with Materials and Atoms, 129, 266–280.
——— (1998) Recoil—Mössbauer spectral analysis software for Windows, version 1.0, pp. 43. University of Ottawa, Canada.
Recoil − Mössbauer spectral analysis software for Windows, K Lagarec and DG Rancourt, Department of Physics, , 1998, version 1.0, pp. 43.
Li, F., Geng, D., and Cao, Q. (2015) Adsorption of As(V) on aluminum-, iron-, and manganese-(oxyhydr)oxides: Equilibrium and kinetics. Desalination and Water Treatment, 56, 1829–1838.
Maillot, F., Morin, G., Wang, Y., Bonnin, D., Ildefonse, P., Chaneac, C., and Calas, G. (2011) New insight into the structure of nanocrystalline ferrihydrite: EXAFS evidence for tetrahedrally coordinated iron(III). Geochimica et Cosmochimica Acta, 75, 2708–2720.
Manceau, A. (2011) Critical evaluation of the revised akdalaite model for ferrihydrite. American Mineralogist, 96, 521–533.
Michel, F.M., Ehm, L., Antao, S.M., Lee, P.L., Chupas, P.J., Liu, G., Strongin, D.R., Schoonen, M.A.A., Phillips, B.L., and Parise, J.B. (2007) The structure of ferrihydrite, a nanocrystalline material. Science, 316, 1726–1729.
Michel, F.M., Barrón, V., Torrent, J., Morales, M.P., Serna, C.J., Boily, J.-F., Liu, Q., Ambrosini, A., Cismasu, A.C., and Brown, G.E. (2010) Ordered ferrimagnetic form of ferrihydrite reveals links among structure, composition, and magnetism. Proceedings of the National Academy of Sciences, 107, 2787–2792.
Mørup, S. (1990) Mössbauer effect in small particles. Hyperfine Interactions, 60, 959–973.
Murad, E. (1988) The Mössbauer spectrum of "well"-crystallized ferrihydrite. Journal of Magnetism and Magnetic Materials, 74, 153–157.
——— (2010) Mössbauer spectroscopy of clays, soils and their mineral constituents. Clay Minerals, 45, 413–430.
——— (2013) Mössbauer spectroscopy, chapter 2.1. In F. Bergaya and G. Lagaly, Eds., Developments in Clay Science, vol. 5, p. 11–24. Elsevier.
Pankhurst, Q., and Pollard, R. (1992) Structural and magnetic properties of ferrihydrite. Clays and Clay Minerals, 40, 268–272.
Peak, D., and Regier, T. (2012) Direct observation of tetrahedrally coordinated Fe(III) in ferrihydrite. Environmental Science & Technology, 46, 3163–3168.
Prescher, C., McCammon, C., and Dubrovinsky, L. (2012) MossA: a program for analyzing energy-domain Mössbauer spectra from conventional and synchrotron sources. Journal of Applied Crystallography, 45, 329–331.
Rancourt, D.G., and Ping, J.Y. (1991) Voigt-based methods for arbitrary-shape static hyperfine parameter distributions in Mössbauer spectroscopy. Nuclear Instruments and Methods in Physics Research Section B: Beam Interactions with Materials and Atoms, 58, 85–97.
Rancourt, D.G., Dang, M.Z., and Lalonde, A.E. (1992) Mössbauer spectroscopy of tetrahedral Fe^{3+} in trioctahedral micas. American Mineralogist, 77, 34–43.
Sassi, M., Chaka, A.M., and Rosso, K.M. (2021) Ab initio thermodynamics reveals the nanocomposite structure of ferrihydrite. Communications Chemistry, 4, 134.
Schwertmann, U., and Cornell, R.M. (2000) Iron Oxides in the Laboratory. Wiley.
Schwertmann, U., Wagner, F., and Knicker, H. (2005) Ferrihydrite–humic associations: Magnetic hyperfine interactions. Soil Science Society of America Journal, 69, 1009–1015.
Swanner, E.D., Wu, W., Schoenberg, R., Byrne, J., Michel, F.M., Pan, Y., and Kappler, A. (2015) Fractionation of Fe isotopes during Fe(II) oxidation by a marine photoferrotroph is controlled by the formation of organic Fe-complexes and colloidal Fe fractions. Geochimica et Cosmochimica Acta, 165, 44–61.
ThomasArrigo, L.K., Byrne, J.M., Kappler, A., and Kretzschmar, R. (2018) Impact of organic matter on iron(II)-catalyzed mineral transformations in ferrihydrite–organic matter coprecipitates. Environmental Science & Technology, 52, 12316–12326.
Tronc, E., Ezzir, A., Cherkaoui, R., Chanéac, C., Noguès, M., Kachkachi, H., Fiorani, D., Testa, A., Greneche, J., and Jolivet, J. (2000) Surface-related properties of γ-Fe_2O_3 nanoparticles. Journal of Magnetism and Magnetic Materials, 221, 63–79.
Weatherill, J.S., Morris, K., Bots, P., Stawski, T.M., Janssen, A., Abrahamsen, L., Blackham, R., and Shaw, S. (2016) Ferrihydrite formation: The role of Fe_{13} Keggin clusters. Environmental Science & Technology, 50, 9333–9342.
Zhao, J., Huggins, F.E., Feng, Z., and Huffman, G.P. (1994) Ferrihydrite: Surface structure and its effects on phase transformation. Clays and Clay Minerals, 42, 737–746.
Zhou, Z., Latta, D.E., Noor, N., Thompson, A., Borch, T., and Scherer, M.M. (2018) Fe(II)-catalyzed transformation of organic matter–ferrihydrite coprecipitates: A closer look using Fe isotopes. Environmental Science & Technology, 52, 11142–11150.

Manuscript received September 10, 2020
Manuscript accepted September 1, 2021
Manuscript handled by Janice L. Bishop

Endnote:

[1]Deposit item AM-22-87802, Online Materials. Deposit items are free to all readers and found on the MSA website, via the specific issue's Table of Contents (go to http://www.minsocam.org/MSA/AmMin/TOC/2022/Aug2022_data/Aug2022_data.html).